ELSEVIER

The role of vacancy defects and holes in the fracture of carbon nanotubes

Steven L. Mielke [a,*], Diego Troya [a], Sulin Zhang [b], Je-Luen Li [c], Shaoping Xiao [d],
Roberto Car [c], Rodney S. Ruoff [b], George C. Schatz [a,*], Ted Belytschko [b,*]

[a] *Department of Chemistry, Northwestern University, 2145 Sheridan Road, Evanston, IL 60208-3113, USA*
[b] *Department of Mechanical Engineering, Northwestern University, Evanston, IL 60208-3111, USA*
[c] *Department of Chemistry, Princeton University, Princeton, NJ 08544-1009, USA*
[d] *Department of Mechanical and Industrial Engineering and Center for Computer-Aided Design, The University of Iowa,
Iowa City, IA 52242-1527, USA*

Received 16 February 2004; in final form 16 April 2004

Abstract

We present quantum mechanical calculations using density functional theory and semiempirical methods, and molecular mechanics (MM) calculations with a Tersoff–Brenner potential that explore the role of vacancy defects in the fracture of carbon nanotubes under axial tension. These methods show reasonable agreement, although the MM scheme systematically underestimates fracture strengths. One- and two-atom vacancy defects are observed to reduce failure stresses by as much as ∼26% and markedly reduce failure strains. Large holes – such as might be introduced via oxidative purification processes – greatly reduce strength, and this provides an explanation for the extant theoretical–experimental discrepancies.
© 2004 Published by Elsevier B.V.

1. Introduction

Carbon nanotubes (CNTs) hold considerable promise as ultra-stiff high-strength fibers for use in cabling and nanocomposites. Several quantum mechanical (QM) studies have reported CNT failure strains in the range of 20–30% and failure stresses usually in excess of 100 GPa [1–5]. (Note that the stress values reported here are obtained using the usual convention that the CNT shell thickness is 3.4 Å.) By contrast, the few direct mechanical measurements [6–9] that have been reported indicate much lower values.

Two sets of measurements [6,8] have been reported for the fracture of ropes of single-walled CNTs (SWCNT), and the maximum failure strains observed were less than 6%. Demczyk et al. [9] reported results for

the fracture of a single multi-walled CNT (MWCNT), that contained 1–5% boron, and which indicated a modulus of 0.91 TPa, a failure strain of $5 \pm 2\%$, and a failure stress of 150 ± 45 GPa. This large failure stress is not consistent with the modulus and strain measurements, and may indicate a measure of interlayer load transfer, possibly resulting from interlayer defects introduced by high-energy transmission electron microscopy (TEM) imaging. Theoretical calculations have already predicted such defects [10,11].

The most extensive set of CNT fracture measurements was reported by Yu et al. [7], and consisted of data for 19 MWCNTs placed under axial tension. The observed failure strains ranged from 2 to 13%, the Young's modulus ranged from 0.27 to 0.95 TPa, and the failure stresses ranged from 11 to 63 GPa, with an average value of 28 GPa. It was subsequently reported [12] that slippage at the cantilever-nanotube attachments might have occurred, which would mean that the modulus and failure-strain measurements can only be regarded as lower and upper bounds, respectively. The

* Corresponding authors. Fax: +1-8474917713.
E-mail addresses: slmielke@chem.northwestern.edu (S.L. Mielke), schatz@chem.northwestern.edu (G.C. Schatz), tedbelytschko@northwestern.edu (T. Belytschko).

failure stresses were independently measured, so these data did not suffer from such possible complications. A plot of the experimental [7] failure-stress distribution is displayed in Fig. 1.

Most attempts to resolve the theoretical–experimental discrepancies have concentrated on the possible role of defects in limiting peak strengths, and the Stone–Wales (SW) defect [13], i.e., a bond rotation that transforms four hexagonal rings into two pentagons and two heptagons, has received the most consideration. (We note that as originally presented, a 'Stone–Wales transformation' referred to the rotation of a bond shared by two adjacent hexagons in icosahedral C_{60}, and which results in an unfavorable conformation having two adjacent pentagons; thus, the usage of the term in the CNT literature is a slight generalization of the original usage.) Electronic structure calculations have indicated that the formation of SW defects becomes energetically favorable at ∼5–6% strain [14–16] for armchair CNTs and at ∼12% strain [16] for zig-zag CNTs. Furthermore, calculations have shown that such defects can bifurcate and migrate along the tube, and that aggregation of defects becomes energetically favorable at high strains [17].

Yakobson [18] proposed that aggregations of SW defects could be followed by a ring-opening mechanism that would permit the nucleation of a crack. Molecular dynamics (MD) simulations using one of the three empirical bond-order potentials of Brenner and co-workers [19,20], and conducted at very high temperatures, have noted substantial weakening from stress-induced SW transformations [21,22], and thus seemingly provided support for this mechanism. Recently, however, QM calculations [3] have indicated that SW defects – even multiple adjacent and pre-existing ones – do not markedly reduce the failure strains and failure stresses of

CNTs. Thus, in this light it would be useful to re-evaluate kinetic estimates of CNT failure [23,24] based on the rate of stress-induced SW defect formation. It was further observed [3] that the empirical bond-order potentials significantly overestimated the weakening caused by SW defects. This suggests that the results of MD simulations [21,22] with these potentials also need to be re-evaluated. It has also been pointed out [2] that at lower temperatures, i.e., 300 K, the barrier to SW formation is high enough to inhibit stress-induced SW defect formation, and that other mechanisms likely prevail for tensile failure of pristine tubes.

We now focus attention on other defects that might result in greater weakening than SW rotations. Mechanisms for CNT growth have been the subject of much discussion [25], but are still poorly understood. Thus, little is known about the types of defects that might be introduced during nanotube synthesis, but vacancy defects, i.e., defects resulting from missing carbon atoms, are likely candidates. These defects have already received considerable attention [10,11,26], in part because they can be readily induced by either electron or ion irradiation, but their effect on tensile strength is not yet known. In this Letter, we present calculations of mechanical properties of CNTs containing one- or two-atom vacancies, and show that while these defects do cause greater weakening than SW defects, they cannot account for the large differences between theory and experiment. We also show that holes *can* result in failure stresses that are low enough to be consistent with the measurements of Yu et al. [7], and we further suggest that such holes were likely introduced by an oxidative purification process.

2. Methodology

Calculations were done using three different approaches. A few calculations were performed using density functional theory (DFT) within the generalized gradient approximation (GGA) [27]. The wavefunctions were expanded in a plane-wave basis set with a 40 Rydberg energy cutoff. From ∼120 to ∼160 carbon atoms in a unit cell within periodic boundary conditions (PBCs) were used with the exact number depending on the defects present. A cell size of 13.8 Å by 13.8 Å was used for the coordinates perpendicular to the axial direction, and a single **k**-space point was used in the Brillouin zone sampling.

A larger set of results was obtained via semiempirical QM calculations with the PM3 [28] approach. These calculations used finite tubes consisting of from ∼170 (for the [5,5] tubes) to ∼200 (for the [10,0] tubes) carbon atoms that were capped at the edges by hydrogen atoms. Strains were applied by varying the axial coordinates of the carbons at the edges of the tube, which were con-
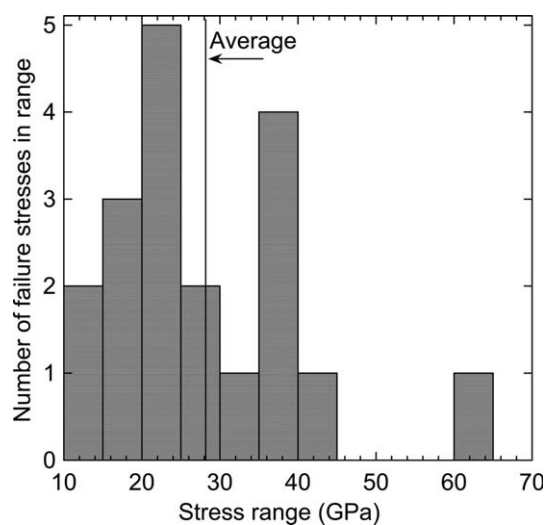

Fig. 1. The failure-stress distribution for the 19 MWCNTs included in the fracture study of Yu et al. [7].

strained to lie within a plane perpendicular to the tube axis. The other coordinates of the edge carbons and all coordinates of the hydrogens and other carbons were then optimized at each applied strain. This is a modification of a procedure used in a prior study that constrained all coordinates of the edge carbons as well as the neighboring hydrogens [3]. For the pristine (undefected) [5,5] tube, additional care was required to avoid fracture at the edges as had happened in the prior study [3]. For this case, we constrained the axial coordinates of the two last planes of carbon atoms at each edge of the tube so that the distance between nearest neighbors of the two planes was ∼1.75 Å for all strain calculations.

Finally, an empirical bond-order potential [20], modified to be appropriate for fracture following a suggestion of Shenderova et al. [29], and denoted MTB-G2 (modified Tersoff–Brenner potential of the second generation), was used for the largest set of calculations. The modified potential removes the cutoff function that reduces to zero the pair interactions over the range 1.7–2.0 Å, *but* retains forces only for those atom pairs that are *initially* less than 2 Å apart. Prior calculations [30,31] that retained this cutoff function obtained qualitatively incorrect fracture properties, including failure stresses for CNTs that were above 300 GPa. The cause of this anomalous behavior has been discussed in more detail elsewhere [3,12,29]. All the MTB-G2 calculations used PBCs. In order to ascertain any dependence of the mechanical properties on tube length, the [5,5] and [10,10] tubes were considered with ∼180 and ∼200 carbons, respectively, to roughly match the lengths used in the PM3 calculations, and we also considered very long tubes (with more than 2500 carbons). The calculations with the [50,0], [29,29], and [100,0] tubes used ∼5000, ∼4988, and ∼10 000 atoms, respectively.

For all three methods, energies were optimized for fixed strain values. The reported stress values are calculated by dividing the force by the product of the current value of the tube circumference and the shell thickness (3.4 Å). Typically, the unstrained configuration was calculated first and then strain was applied in small steps. The starting configuration for each optimization was usually taken from the optimized value obtained with the previous (and lower) strain, although in certain cases additional fracture paths were mapped out using alternative schemes (usually by contracting from larger-strain configurations or departing from partially symmetrized configurations).

3. Results and discussion

We begin by considering pristine tubes and the effects that one- and two-atom vacancies can have on their mechanical properties. If a single atom is removed from the lattice, a 12-membered ring results and this can re-

construct to a five-membered ring and a nine-membered ring in one of two unique ways. For both armchair and zig-zag CNTs, these reconstructions result in one symmetric configuration and one asymmetric configuration. If two adjacent carbons are missing, the resulting 14-membered ring can reconstruct to form two pentagons and an octagon; this also leads to two unique defect patterns for either zig-zag or armchair tubes. Fig. 2 illustrates these reconstructed defect patterns. All carbon atoms in the reconstructed double-vacancy structures are saturated so these structures are expected to be reasonably stable. The reconstructed single-vacancy structures contain one unsaturated carbon and thus will be more reactive. At high temperatures the single vacancies can migrate around the tube [26] and possibly combine with other single vacancies on the same tube to form the more stable double-vacancy structures, or combine with vacancies on adjacent tubes to form bridged structures [10], or merely react with other species such as O_2 (if exposed to air).

Table 1 lists the radii, Young's moduli, failure stresses, and failure strains of all of the pristine tubes considered here as predicted by the three different methods as well as the recent DFT calculations of Ogata and Shibutani [4].

[5,5] 1 at. sym.   **[5,5] 1 at. asym.**

[5,5] 2 at. sym.   **[5,5] 2 at. asym.**

[10,0] 1 at. sym.   **[10,0] 1 at. asym.**

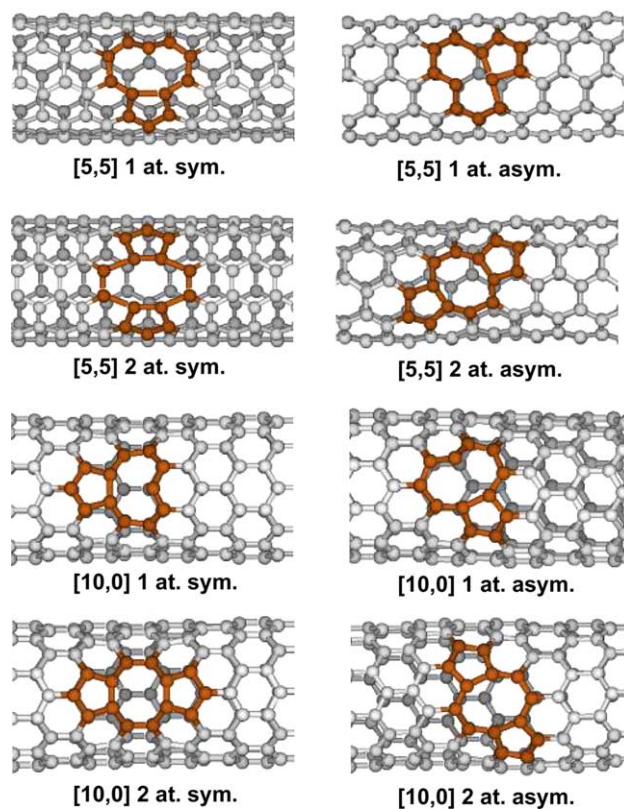**[10,0] 2 at. sym.**   **[10,0] 2 at. asym.**

Fig. 2. The reconstructions of the one- and two-atom vacancy defects considered here.

Table 1
Mechanical properties of pristine CNTs

Method	Tube	Radius (Å)	Young's modulus (TPa)	Failure stress (GPa)	Failure strain
DFT (present)	[5,5]	3.43	0.96	110	0.30
DFT (Ogata and Shibutani)[a]	[8,8]	n/a	1.01	115	0.295
PM3	[5,5]	3.43	1.1	135	0.30
MTB-G2	[5,5]	3.43	0.78	105	0.297
DFT (present)	[10,0]	3.95	0.94	105	0.20
DFT (Ogata and Shibutani)	[10,0]	n/a	0.97	107	0.208
PM3	[10,0]	3.94	1.1	124	0.20
MTB-G2	[10,0]	3.97	0.92	88	0.181
MTB-G2	[29,29]	19.68	0.72	102	0.239
MTB-G2	[50,0]	19.59	0.85	88.8	0.189
MTB-G2	[100,0]	39.16	0.84	88.9	0.188

[a] Note that the only armchair tube considered by Ogata and Shibutani [4] was an [8,8].

The moduli predicted by PM3 are slightly larger than those of the DFT calculations, while the MTB-G2 scheme predicts lower values. Additionally, while both PM3 and DFT give quite similar values for zig-zag and armchair tubes, the MTB-G2 moduli seem to converge with increasing radii to different limits for these two cases, with the zig-zag tubes being about 18% stiffer. In the large-radius limit, the moduli should approach the *isotropic* graphene limit of ∼1.06 TPa; thus, this behavior of the MTB-G2 potential is a significant artifact of the empirical methodology.

The failure strains of the pristine tubes calculated by all the methods show remarkable agreement. The failure stresses of the DFT results of Ogata and Shibutani [4] are in excellent agreement with the present DFT calculations, while the PM3 results are about 20% higher and the MTB-G2 values are 5% lower for the [5,5] case and 16% lower for the [10,0] case.

Fig. 3 displays the stress–strain curves for pristine [10,0] and [5,5] CNTs as well as two defective tubes calculated by DFT, PM3, and MTB-G2. The structure of the [5,5] stress–strain curve is especially complex, with several distinct equilibrium pathways observed in the two QM calculations. At the highest strains both the DFT and PM3 solutions consist approximately of uniform stretching of all axially aligned bonds. At the lower strains (<17%), the DFT solution again exhibits uniform stretching, but along a path that does not connect with the path observed at high strains. Similar behavior has also been observed by Ogata and Shibutani [4]. A third DFT pathway was observed at strains in the neighborhood of 17% which involved unequal bond stretching with lower energies than the other pathways. A larger number of pathways were mapped out with the PM3 method. The unstrained PM3 structure displays an alternating bond-length pattern for the axially aligned bonds, as do all of the lower-strain pathways. As the tube is incrementally stretched along a given pathway, the deviations in these bond lengths increase significantly. Different degrees of distortion are present in the

different pathways, and the lowest-energy path invariably corresponded to the lowest-stress solution for a given strain. Mapping out all of the pathways was not unfeasible, and the associated barriers between paths were not studied. The physically relevant pathways may depend on the time scale, the temperature, etc.; in the following we will assume that transitions between pathways are readily achieved, and thus that the higher-strain solutions are accessible. Ogata and Shibutani [4] expressed a belief that the higher-strain solutions were 'unstable' because they were not observed during optimizations at constant stress, but it is also possible that the high-stress solutions at intermediate strains are the unstable solutions.

The DFT and PM3 methods show good agreement for the predicted failure strains of defective tubes. The two methods also agree well for the fractional stress reductions with PM3 indicating a 19% reduction for a single vacancy in a [10,0] CNT and an 18% reduction for the case of an asymmetric double vacancy in a [5,5] CNT while DFT predicts reductions of 18% and 16%, respectively, for these cases. By contrast, MTB-G2 significantly underestimates the strains and stresses at failure for tubes involving defects. This is consistent with earlier observations [3] that MTB-G2 incorrectly predicted significant weakening from aggregations of SW defects.

Table 2 lists the failure stresses and failure strains for the various vacancy-defected tubes obtained by PM3 and MTB-G2 calculations. Comparison values for pristine tubes and tubes with axially aligned Stone–Wales defects are also given. QM calculations with tubes long enough to have fully converged failure strains are unaffordable, but we considered MTB-G2 calculations with lengths similar to those used in the PM3 calculations as well as long lengths sufficient to converge all properties. The shorter tubes had failure strains that are 1–27% larger than converged values; by contrast, the failure stresses converged quite rapidly with length.
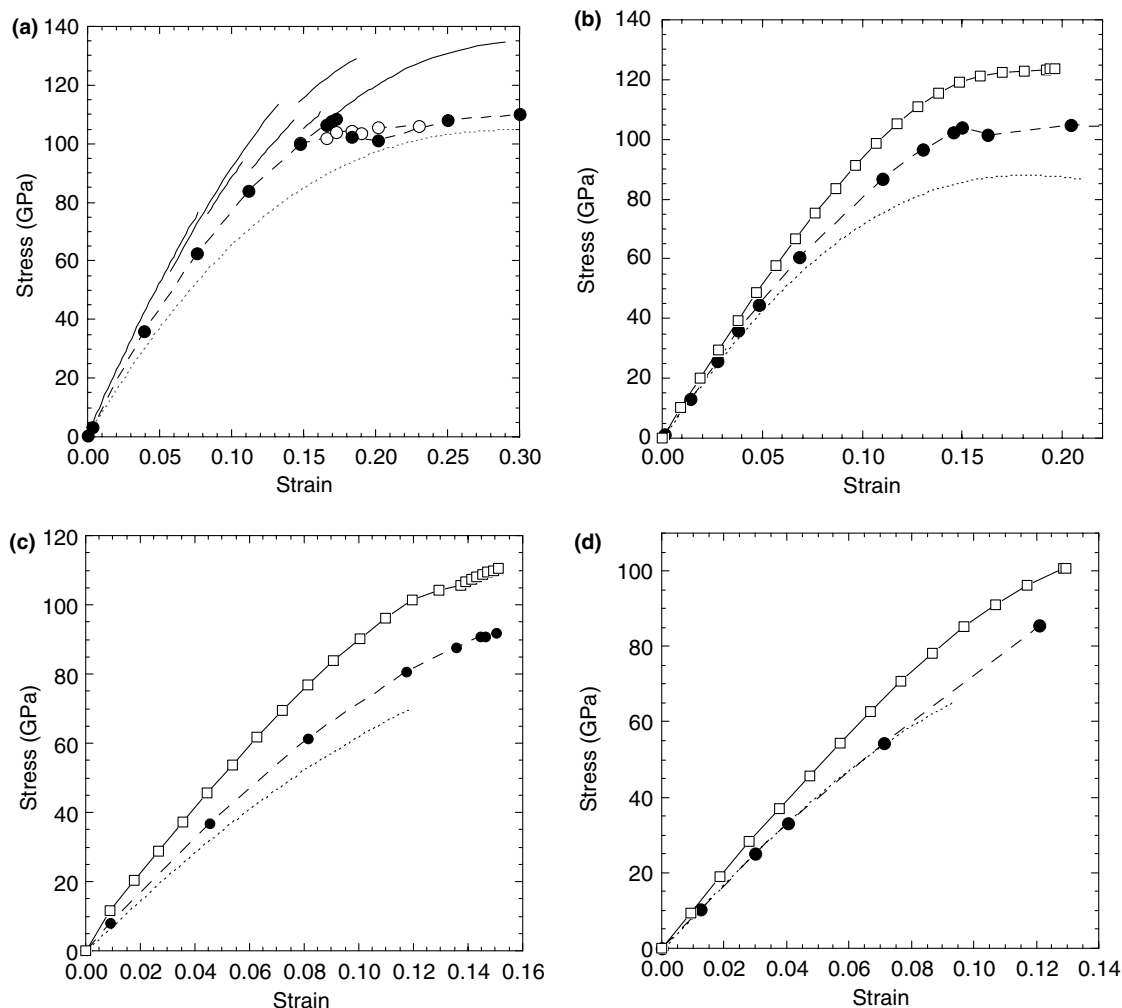
Fig. 3. Stress–strain curves for a selection of tubes calculated via DFT (long dashes), PM3 (solid line), and MTB-G2 (short dashes). (a) Pristine [5,5] CNT; (b) pristine [10,0] CNT; (c) two-atom vacancy (asymmetric configuration) in a [5,5] CNT; and (d) one-atom vacancy in a [10,0] CNT.

Table 2
Failure stresses (GPa) and strains of pristine CNTs and CNTs with axially aligned Stone–Wales defects or one- and two-atom vacancy defects calculated with PM3 and MTB-G2

Tube	Defect	PM3		MTB-G2			
		Stress	Strain	Stress (S)[a]	Stress (L)[b]	Strain (S)	Strain (L)
[10,0]	Pristine	124	0.20	88	88	0.184	0.181
[10,0]	Stone–Wales	115	0.139	72	72	0.110	0.101
[10,0]	One-atom vac.	101	0.130	65	65	0.096	0.087
[10,0]	Two-atom vac. sym.	107	0.142	66	64	0.096	0.085
[10,0]	Two-atom vac. asym.	92	0.124	67	65	0.109	0.089
[5,5]	Pristine	135	0.30	105	105	0.297	0.297
[5,5]	Stone–Wales[c]	125	0.22	89	88	0.175	0.162
[5,5]	One-atom vac.	100	0.153	71	71	0.131	0.115
[5,5]	One-atom vac. + H sym.	106	0.149	85	85	0.167	0.152
[5,5]	One-atom vac. + H asym.	99	0.151	71	71	0.132	0.115
[5,5]	Two-atom vac. sym.	105	0.172	72	71	0.149	0.117
[5,5]	Two-atom vac. asym.	111	0.152	70	73	0.120	0.119

[a] (S) indicates a short tube with a length similar to that used in the PM3 calculations.

[b] (L) indicates a long tube.

[c] Ref. [3].

If the unsaturated orbitals of the single vacancies are not terminated with other species such as hydrogen, then the two configurations where the new pentagon bond formed along the axial direction (the symmetric configuration for the [5,5] case and the asymmetric configuration for the [10,0] case) rearrange to the alternative configuration as the tube is stretched; thus, both configurations have the same fracture properties. If, instead, we saturate the half-filled orbital with a hydrogen atom, the axially aligned bond can be maintained and the resulting tubes are slightly stronger. The PM3 calculations indicate that the various one- and two-atom vacancies reduce the failures stresses by 14–26% and markedly reduce the failure strains – by about a factor of two for armchair tubes. The defects that cause the greatest fractional stress reductions are the asymmetric single vacancy for the [5,5] tube (26% reduction), and the two-atom asymmetric vacancy for the [10,0] tube (26% reduction) where both of the weak bonds resulting from the reconstruction are axially aligned. The vacancy defect that results in the smallest fractional stress reduction (14%) is the symmetric two-atom vacancy in the [10,0] tube where both of the weak bonds resulting from the reconstruction are oriented perpendicular to the tube axis. The MTB-G2 potential predicts significantly lower failure strains and stresses than the PM3 calculations do. The MTB-G2 potential is also quite insensitive to the effect of orientation on the failure stresses; for instance, it predicts that the failure stresses of the symmetric and asymmetric configurations of the two-atom vacancy in the [10,0] tube differ by 1 GPa, whereas the PM3 results differ by 15 GPa.

While fractional stress reductions of 26% are significant, they are far from what would be required to explain the discrepancies between the experimental results and theoretical predictions. Apparently, only very significant defects can account for these discrepancies. The preparation and purification approach [32] of the MWCNTs used in the experiments of Yu et al. [7] included an oxidative etching for 30 min in an air stream at 650 °C. The highly defected tubes, soot, and other impurities – which constituted the bulk of the material – were rapidly removed by this process and only well-formed MWCNTs remained. However, even well-formed CNTs may be expected to have an occasional vacancy defect, and thus would also be partially vulnerable to oxidation. Oxidative pitting of the basal plane of graphite by O [33] and O_2 [34,35] has already been extensively studied under similar conditions. Oxidation begins at the sites of vacancy defects and rapidly etches roughly circular holes in the uppermost graphene sheet. It is thus very likely that the tubes used in the mechanical measurements of Yu et al. [7] contained large holes in the load-bearing outer shell, but these defects would not have been detectable via the TEM imaging used to examine them, or the scanning electron microscopy used during the tensile loading experiments.

We next consider the effect that such holes might have on the mechanical properties. We will consider a systematic series of increasingly large holes beginning with the removal of an entire hexagonal ring (six carbons removed), then removing the six hexagons around this hexagon (18 additional carbons removed), then removing the neighboring 12 hexagonal rings, etc. It will be convenient to denote the size of the hole via an index with the original six-atom excision being an index of 0, and the other holes having an index specifying the number of additional rings of hexagons that have been excised. We saturate the system with hydrogens since an empirical bond-order potential is not yet available for oxygen. The effect of small holes on the strength of CNTs has already been considered by Hirai et al. [31], but the retention of the cutoff functions in the bond-order potential rendered the results unphysical.

For both armchair and zig-zag tubes, the index 0 hole removes two axial bonds, and each increment results in an additional pair of axial bonds being severed. We also considered one hole intermediate between the index 0 and index 1 holes that involved removing only the six carbons closest to the ring excised in the index 0 hole; this case removes two additional axial bonds for the armchair tubes but none for zig-zag tubes. We conducted PM3 and MTB-G2 calculations for [5,5] and [10,0] tubes with the index 0 hole, this intermediate-sized hole, and the index 1 hole; the results are presented in Table 3. The QM failure stresses with these three holes are 75%, 56%, and 58%, respectively, of the pristine failure stress value for the armchair tube, and 72%, 68%, and 54%, respectively, of the pristine failure stress value for the zig-zag case. In each case, this corresponds to failure-stress reductions that are several percent higher than what would be predicted based solely on the fraction of excised axial bonds. The MTB-G2 results overestimate the weakening effect of the holes in all cases.

We note that while the molecular mechanics (MM) calculations significantly under-predict failure stresses of

Table 3
Failure stresses (GPa) of small tubes with holes calculated with PM3 and MTB-G2

Hole size index[a]	PM3	Short tube MTB-G2	Long tube MTB-G2
[5,5] pristine	135	105	105
[5,5] index 0	101	70	68
[5,5] intermediate	76	50	47
[5,5] index 1	78	53	50
[10,0] pristine	124	88	88
[10,0] index 0	89	56	52
[10,0] intermediate	84	56	46
[10,0] index 1	67	42	36

[a] See text for the hole-size classification scheme.

Table 4
Failure stresses (GPa) and strains of large CNTs with holes calculated with the MTB-G2 potential

Hole size index[a]	[50,0]		[100,0]		[29,29]	
	Stress	Strain	Stress	Strain	Stress	Strain
Pristine	88.8	0.189	88.9	0.188	101.5	0.239
0	57.7	0.075	58.2	0.076	76.8	0.129
1	45.6	0.058	47.3	0.060	62.2	0.098
2	39.7	0.051	42.2	0.053	53.8	0.083
3	35.9	0.048	38.9	0.050	48.3	0.076
4	33.2	0.046	36.7	0.048	44.8	0.072
5	31.3	0.045	35.1	0.046	42.4	0.071

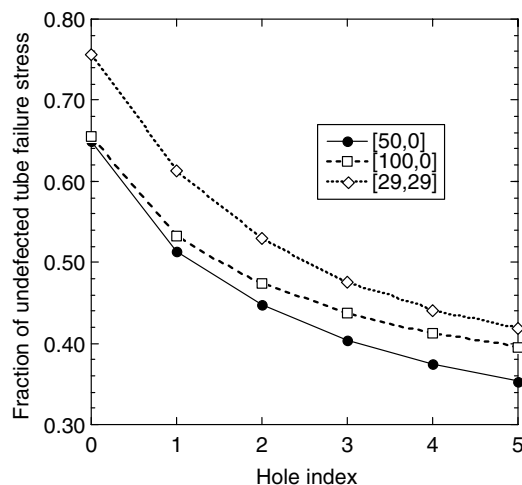[a] See text for the hole-size classification scheme.

Fig. 4. The ratio of the failure stress of a CNT with a hole (see text for the definition of the hole-size index) to the failure stress of the corresponding pristine CNT as a function of the hole size as calculated using the MTB-G2 empirical bond-order potential.

defective nanotubes, the fractional reductions for various defects is good enough to provide some insight into the effects of larger defects. Therefore, we considered much larger tubes where only calculations with the MTB-G2 potential were affordable: a [50,0] tube and an armchair tube of approximately the same radius, [29,29], and also a [100,0] tube to demonstrate that the trends do not vary greatly with additional increases in the tube radius. These results are displayed in Table 4, and a plot of the fractional stresses vs. hole size is presented in Fig. 4. These data clearly indicate that very large strength reductions in large tubes can be caused by moderately sized holes.

4. Concluding remarks

We have explored the role that missing atoms have in the fracture of defected carbon nanotubes (CNTs). The predictions of semiempirical and density functional theory calculations show reasonable agreement, but a more affordable, and widely used, empirical bond-order potential of Brenner et al. [20] systematically underestimates the mechanical properties of defected CNTs. Large, approximately circular, holes which would be consistent with damage resulting from harsh oxidative purification processes are observed to substantially reduce the failure stresses and failure strains of CNTs and provide a likely explanation for the discrepancy between prior mechanical measurements and theoretical predictions. One- and two-atom vacancy defects, which may be expected to occasionally occur during most synthetic schemes or be introduced during measurements conducted via high-energy TEM imaging, are observed to reduce the failure stresses of pristine tubes by as much as 26% and to reduce the expected failure strains by as much as a factor of two. These reductions are much larger than those caused by Stone–Wales defects; thus, vacancy defects may be the strength-limiting defect for high-quality CNTs.

References

[1] T. Ozaki, Y. Iwasa, T. Mitani, Phys. Rev. Lett. 84 (2000) 1712.
[2] T. Dumitrica, T. Belytschko, B.I. Yakobson, J. Chem. Phys. 118 (2003) 9485;
J. Chem. Phys. 119 (2003) 1281E.
[3] D. Troya, S.L. Mielke, G.C. Schatz, Chem. Phys. Lett. 382 (2003) 133.
[4] S. Ogata, Y. Shibutani, Phys. Rev. B 68 (2003) 165409.
[5] G. Dereli, C. Ozdogan, Phys. Rev. B 67 (2003) 035416.
[6] D.A. Walters, L.M. Ericson, M.J. Casavant, J. Liu, D.T. Colbert, K.A. Smith, R.E. Smalley, Appl. Phys. Lett. 74 (1999) 3803.
[7] M.-F. Yu, O. Lourie, M.J. Dyer, K. Moloni, T.F. Kelly, R.S. Ruoff, Science 287 (2000) 637.
[8] M.-F. Yu, B.S. Files, S. Arepalli, R.S. Ruoff, Phys. Rev. Lett. 84 (2000) 5552.
[9] B.G. Demczyk, Y.M. Wang, J. Cumings, M. Hetman, W. Han, A. Zettl, R.O. Ritchie, Mater. Sci. Eng. A 334 (2002) 173.
[10] R.H. Telling, C.P. Ewels, A.A. El-Barbary, M.I. Heggie, Nat. Mater. 2 (2003) 333.
[11] A.V. Krasheninnikov, K. Nordlund, J. Keinonen, Phys. Rev. B 65 (2002) 165423.
[12] T. Belytschko, S.P. Xiao, G.C. Schatz, R.S. Ruoff, Phys. Rev. B 65 (2002) 235430.
[13] A.J. Stone, D.J. Wales, Chem. Phys. Lett. 128 (1986) 501.
[14] M.B. Nardelli, B.I. Yakobson, J. Bernholc, Phys. Rev. B 57 (1998) R4277.
[15] Q. Zhao, M.B. Nardelli, J. Bernholc, Phys. Rev. B 65 (2002) 144105.

[16] P. Zhang, P.E. Lammert, V.H. Crespi, Phys. Rev. Lett. 81 (1998) 5346.

[17] M.B. Nardelli, B.I. Yakobson, J. Bernholc, Phys. Rev. Lett. 81 (1998) 4656.

[18] B.I. Yakobson, Appl. Phys. Lett. 72 (1998) 918.

[19] D.W. Brenner, Phys. Rev. B 42 (1990) 9458; Phys. Rev. B 46 (1992) 1948E.

[20] D.W. Brenner, O.A. Shenderova, J.A. Harrison, S.J. Stuart, B. Ni, S.B. Sinnott, J. Phys.: Condens. Matter 14 (2002) 783.

[21] C. Wei, K. Cho, D. Srivastava, Phys. Rev. B 67 (2003) 115407.

[22] C. Wei, K. Cho, D. Srivastava, Appl. Phys. Lett. 82 (2003) 2512.

[23] G.G. Samsonidze, G.G. Samsonidze, B.I. Yakobson, Phys. Rev. Lett. 88 (2002) 065501.

[24] G.G. Samsonidze, G.G. Samsonidze, B.I. Yakobson, Comput. Mater. Sci. 23 (2002) 62.

[25] J.-C. Charlier, S. Iijima, Top. Appl. Phys. 80 (2001) 55.

[26] P.M. Ajayan, V. Ravikumar, J.-C. Charlier, Phys. Rev. Lett. 81 (1998) 1437.

[27] J.P. Perdew, K. Burke, M. Ernzerhof, Phys. Rev. Lett. 77 (1996) 3865; Phys. Rev. Lett. 78 (1997) 1396E.

[28] J.J.P. Stewart, J. Comput. Chem. 10 (1989) 209.

[29] O.A. Shenderova, D.W. Brenner, A. Omeltchenko, X. Su, L.H. Yang, Phys. Rev. B 61 (2000) 3877.

[30] B.I. Yakobson, M.P. Cambell, C.J. Brabec, J. Bernholc, Comput. Mater. Sci. 8 (1997) 341.

[31] Y. Hirai, S. Nishimaki, H. Mori, Y. Kimoto, S. Akita, Y. Nakayama, Y. Tanaka, Jpn. J. Appl. Phys. 42 (2003) 4120.

[32] D.T. Colbert, J. Zhang, S.M. McClure, P. Nikolaev, Z. Chen, J.H. Hafner, D.W. Owens, P.G. Kotula, C.B. Carter, J.H. Weaver, A.G. Rinzler, R.E. Smalley, Science 266 (1994) 1218.

[33] K.T. Nicholson, T.K. Minton, S.J. Sibener, Prog. Org. Coatings 47 (2003) 443.

[34] R.T. Yang, C. Wong, Science 214 (1981) 437.

[35] S.M. Lee, Y.H. Lee, Y.G. Hwang, J.R. Hahn, H. Kang, Phys. Rev. Lett. 82 (1999) 217.